



HAL
open science

Transient translation symmetry breaking via quartic-order negative light-phonon coupling at the Brillouin zone boundary in KTaO_3

Adrián Gómez Pueyo, Alaska Subedi

► **To cite this version:**

Adrián Gómez Pueyo, Alaska Subedi. Transient translation symmetry breaking via quartic-order negative light-phonon coupling at the Brillouin zone boundary in KTaO_3 . *Physical Review B*, 2023, 108 (6), pp.064302. 10.1103/PhysRevB.108.064302 . hal-04307875

HAL Id: hal-04307875

<https://hal.science/hal-04307875>

Submitted on 27 Feb 2024

HAL is a multi-disciplinary open access archive for the deposit and dissemination of scientific research documents, whether they are published or not. The documents may come from teaching and research institutions in France or abroad, or from public or private research centers.

L'archive ouverte pluridisciplinaire **HAL**, est destinée au dépôt et à la diffusion de documents scientifiques de niveau recherche, publiés ou non, émanant des établissements d'enseignement et de recherche français ou étrangers, des laboratoires publics ou privés.

Transient translation symmetry breaking via quartic-order negative light-phonon coupling at the Brillouin zone boundary in KTaO_3

Adrián Gómez Pueyo and Alaska Subedi

CPHT, CNRS, Ecole Polytechnique, IP Paris, F-91128 Palaiseau, France

(Dated: August 2, 2023)

KTaO_3 presents a rich hyper-Raman spectrum originating from two-phonon processes at the Brillouin zone boundary, indicating the possibility of driving these phonon modes using intense midinfrared laser sources. We obtained the coupling of light to the highest-frequency longitudinal optic phonon mode Q_{HY} at the X $(0, 0, \frac{1}{2})$ point by first principles calculations of the total energy as a function of the phonon coordinate Q_{HY} and electric field E . We find that the energy curve as a function of Q_{HY} softens for finite values of electric field, indicating the presence of $Q_{\text{HY}}^2 E^2$ nonlinearity with negative coupling coefficient. We studied the feasibility of utilizing this nonlinearity to transiently break the translation symmetry of the material by making the Q_{HY} mode unstable with an intense midinfrared pump pulse. We also considered the possibility that nonlinear phonon-phonon couplings can excite the lowest-frequency phonon coordinates Q_{LZ} and Q_{LX} at X when the Q_{HY} mode is externally driven. The nonlinear phonon-phonon couplings were also obtained from first principles via total-energy calculations as a function of the phonon coordinates, and these were used to construct the coupled classical equations of motion for the phonon coordinates in the presence of an external pump term on Q_{HY} . We numerically solved them for a range of pump frequencies and amplitudes and found three regimes where the translation symmetry is broken: i) rectification of the lowest-frequency coordinates due to large amplitude oscillation of the Q_{HY} coordinate about its equilibrium position, ii) rectification of only the Q_{HY} coordinate without displaced oscillations of the lowest-frequency coordinates, and iii) rectification of all three coordinates. Due to the small magnitude of the coupling constant between the Q_{HY} mode and the electric field, the smallest value of the pump amplitude that manages to transiently break the translation symmetry of KTaO_3 is 270 MV/cm. Such a large value of electric field will likely cause a dielectric breakdown of the material. However, our paper shows that light-phonon coupling with negative sign can exist in real materials and motivates the search of other materials with a larger magnitude of the coupling.

I. INTRODUCTION

Light-induced amorphous-crystalline phase change in $\text{Ge}_2\text{Sb}_2\text{Te}_5$ [1] and transition to a hidden state in $1T\text{-TaS}_2$ [2] are notable examples of structural control of materials using light. Recently, it has been realized that a cubic-order nonlinear coupling between a fully-symmetric Raman and an infrared phonon mode at the Brillouin zone center can be used to displace the crystal structure of a material along the Raman phonon coordinate when the infrared phonon mode is externally driven [3]. First principles calculation of nonlinear phonon couplings has been used to propose ultrafast switching of ferroelectrics using this mechanism [4]. Subsequent experiments have observed pump-induced transient reversal of electrical polarization [5, 6], although it has not been clarified whether this is caused by a long-period oscillation of a soft phonon mode or its oscillations at a displaced position. Nonetheless, recent theoretical studies support the nonlinear phonon coupling as a mechanism to explain this transient reversal of ferroelectricity [7–9].

Density functional theory based calculations show that quartic-order $Q_1^2 Q_2^2$ nonlinearity with negative coupling coefficients can occur between two phonon modes Q_1 and Q_2 [10], and this has been used to show that a light-induced transition to a transient ferroelectric state in paraelectric materials is possible [11]. Interestingly, it has been shown that cubic-order couplings can also be used to cause oscillations of a symmetry-breaking Raman

mode at a rectified position when it couples to a doubly degenerate infrared mode [12]. There is experimental indication of a transient symmetry breaking in Bi_2Se_3 after a midinfrared pump [13]. Furthermore, several theoretical studies have highlighted coupling of magnetism to phonon coordinates of a material [14–21], and there are multiple experimental studies that show light-driven phononic alteration of magnetic behavior [22–26]. The aforementioned studies have explored novel pathways for structural control of materials via nonlinear phononics, but they do not involve changes in the size of the crystalline unit cell caused by breaking the translation symmetry of the material.

In our previous work [27], we studied a method to transiently break the translation symmetry of a crystal by pumping the highest-frequency transverse optic (TO) phonon mode at the Brillouin zone boundary via a second-order Raman process. We found that the pumped mode can soften the lowest-frequency phonon mode also at the zone boundary due to a quartic-order phonon-phonon coupling with negative coupling constant. When the amplitude of the oscillations of the pumped mode was large enough, the lowest-frequency mode became unstable, thereby breaking the translation symmetry. The role of light in this symmetry-breaking process was limited to the excitation of the highest-frequency TO phonon.

In this paper, we investigate the possibility of transiently breaking the translation symmetry of a material by softening the pumped phonon mode itself. Our

first principles calculations show a $\alpha Q_{\text{HY}}^2 E^2$ nonlinear light-phonon coupling with negative coupling constant between the highest-frequency longitudinal optic (LO) mode Q_{HY} of KTaO_3 and external electric field E , which implies that it is in principle possible to break the translation symmetry of this material by pumping this mode. To identify the peak electric field of the pump pulse required to cause the symmetry breaking, we numerically solved the coupled classical equations of motion of the Q_{HY} and lowest-frequency transverse acoustic (TA) phonon coordinates Q_{LZ} and Q_{LX} . The equations of motion were constructed using the nonlinear light-phonon and phonon-phonon couplings extracted from first principles total-energy calculations. The numerical solutions of these equations yield a set of dynamics of the phonon coordinates that is distinct from our previous study where the highest-frequency TO mode was pumped. We find that the rectification of the driven LO coordinate Q_{HY} requires a pump amplitude of at least 370 MV/cm. Additionally, the rectification of the TA coordinates occurs when the Q_{HY} mode is pumped with a lower pump amplitude of 270 MV/cm. These are very high values of pump intensities that are at least an order of magnitude larger than what can be produced using currently available mid-infrared laser sources. Furthermore, such intense sources may physically damage the samples. Nevertheless, our paper shows that a quartic-order negative light-phonon coupling can occur in real materials, and this can in principle be utilized to break the translation symmetry of a material by softening the pumped mode.

II. THEORETICAL APPROACH

We are interested in the light-induced dynamics of three phonon modes of KTaO_3 at the X ($0, \frac{1}{2}, 0$) point of its Brillouin zone: the highest-frequency LO mode Q_{HY} that is externally pumped and the two components of the lowest-frequency doubly degenerate TA mode Q_{LZ} and Q_{LX} . The nonlinear light-phonon and phonon-phonon couplings were obtained from density functional theory based first principles calculations, and the light-induced dynamics of the system was studied using the methodology presented in Ref. [10]. This approach requires the calculation of the phonon eigenvectors, which are then used to compute the total-energy surface $V(Q_{\text{HY}}, Q_{\text{LX}}, Q_{\text{LZ}})$ as a function of the LO and TA phonon coordinates (see Ref. [28] for a review). The phonon anharmonicities and phonon-phonon nonlinear couplings are then obtained by fitting the total-energy surface with a polynomial. We used the approach previously used by Cartella *et al.* [29] to obtain the coupling between the pumped phonon mode and the laser pulse by calculating the total energy as a function of the Q_{HY} mode and fitting it with a polynomial. The phonon anharmonicities, the phonon-phonon nonlinear couplings, and the light-phonon coupling are used to construct the coupled equations of motion for the phonon coordinates in the presence of an external

force term on the highest-frequency Q_{HY} mode. These are then solved numerically to obtain the structural evolution of the material as a function of time.

First principles calculations of the phonon frequencies and eigenvectors and the total-energy surfaces as a function of the phonon coordinates and electric field were done using the QUANTUM ESPRESSO [30] (QE) package. These were performed within the PBEsol generalized gradient approximation [31] using the ultrasoft pseudopotentials with the valence orbitals $3s^2 3p^6 4s^1$ (K), $5s^2 5p^6 5d^3 6s^1$ (Ta), and $2s^2 2p^4$ (O) from the GBRV library [32]. The plane-wave cutoffs for the basis set and charge density expansions were set to 60 and 600 Ry, respectively. We used the relaxed lattice parameter of $a = 3.98784 \text{ \AA}$ in our calculations. The phonon frequencies and eigenvectors at the Brillouin zone boundary point X were calculated using density functional perturbation theory [33] as implemented in QE. The computation of the dynamical matrix requires a previous self-consistent field calculation, which was performed using an $8 \times 8 \times 8$ Monkhorst-Pack k -point grid.

We then used the calculated phonon eigenvectors to generate modulated structures as a function of the Q_{HY} , Q_{LX} , and Q_{LZ} coordinates in $1 \times 2 \times 1$ supercells and calculated their total energies to extract the phonon anharmonicities and phonon-phonon nonlinear couplings. For the total-energy surfaces calculated as a function of two phonon coordinates, we sampled values ranging from -2.4 to $2.4 \text{ \AA}\sqrt{u}$ with a step size of $0.08 \text{ \AA}\sqrt{u}$ for the TA phonon coordinates Q_{LX} and Q_{LZ} , and from -1.0 to $1.0 \text{ \AA}\sqrt{u}$ with a step size of $0.05 \text{ \AA}\sqrt{u}$ for the LO coordinate Q_{HY} . In the calculations of the total-energy surface as a function of the three phonon coordinates, we sampled values of the TA coordinates ranging from -3.0 to $3.0 \text{ \AA}\sqrt{u}$ with a step size of $0.1 \text{ \AA}\sqrt{u}$, and for the LO coordinate values from -1.0 to $1.0 \text{ \AA}\sqrt{u}$ with a step size of $0.05 \text{ \AA}\sqrt{u}$. These values were chosen to modify the shortest distance between atoms of the crystal at most 10% of their original values, allowing us to explore the anharmonicities of the material while remaining below the Lindemann stability limit [34]. An $8 \times 4 \times 8$ Monkhorst-Pack k -point grid was used in these calculations. The calculated total-energy surfaces were fit with polynomials having only the symmetry-allowed nonlinear terms using the GLM [35] package as implemented in JULIA. Thus obtained phonon anharmonicities and phonon-phonon couplings are given in Appendix B.

The modern theory of polarization [36] as implemented in QE was used to calculate the total-energy surface of KTaO_3 as a function of the highest-frequency Q_{HY} coordinate and electric field E . We sampled the electric field using values ranging from -14.54 to 14.54 MV/cm with a step of 3.635 MV/cm and Q_{HY} ranging from -1.0 to $1.0 \text{ \AA}\sqrt{u}$ with a step of $0.1 \text{ \AA}\sqrt{u}$. A slightly denser $8 \times 8 \times 8$ Monkhorst-Pack k grid was used to sample the Brillouin zone in these calculations. We then fit the

resulting energy surface to the following polynomial:

$$H(Q_{\text{HY}}, E) = \frac{1}{2}\Omega_{\text{HY}}^2 Q_{\text{HY}}^2 + d_4 Q_{\text{HY}}^4 + d_6 Q_{\text{HY}}^6 + d_8 Q_{\text{HY}}^8 + rE + sE^2 + tE^4 + \alpha Q_{\text{HY}}^2 E^2, \quad (1)$$

where the frequency Ω_{HY} and anharmonic coefficients d_i of the Q_{HY} mode are those extracted from the previous total-energy calculations and $s = -1.5386 \text{ e}\text{\AA}^2/\text{V}$, $t = -0.258 \text{ e}\text{\AA}^4/\text{V}^3$, and $\alpha = -0.205 \text{ e}/(\text{V u})$ are the coefficients for the terms allowed by symmetry between the electric field and the Q_{HY} coordinate. We get a finite value of $r = -259.21 \text{ e}\text{\AA}$ for the coefficient of E in $H(Q_{\text{HY}}, E)$, which occurs due to the use of periodic boundary conditions. To validate this method of obtaining light-phonon coupling, we noted in our previous work that the coupling of the electric field to the highest-frequency phonon of KTaO_3 at the Brillouin zone center Γ extracted using this method agrees well with that obtained using the perturbation theory approach, which is implemented in density functional theory codes for phonons at Γ [27]. We are also aware that the largest electric field that we have used in the total-energy calculations is more than an order of magnitude smaller than the values that cause rectification of the phonon coordinates in the numerical solution of the equations of motion. Larger values of the electric field caused oscillations of the total energy during the self-consistent field iterations of density functional calculations. This is a limitation of the currently available computational method.

The DIFFERENTIALEQUATIONS [37] package from the JULIA language was used to integrate the coupled differential equations of motion, which was carried out using the strong stability preserving method of Ruuth. The time range for the propagation was from 0 to 8 ps, and the peak amplitude of the laser pulse was reached at 4 ps. The initial conditions were set such that $Q_{\text{HY}} = Q_{\text{LX}} = Q_{\text{LZ}} = 0.1 \text{ \AA}\sqrt{\text{u}}$ and their first derivative with respect to time equal to zero. We added a stochastic term in the form of white noise from the start of the propagation until the peak of the pump pulse to simulate the thermal fluctuations of the phonons [38, 39]. To implement this, we picked a random value from a flat distribution going from -1 to 1 and then multiplied it by a scaling factor to make it comparable to the amplitude of the initial conditions for each mode. This scaling factor is different for the high- and low-frequency modes, as their damping coefficients are also different. For Q_{HY} we used $300/N$ and for Q_{LX} and Q_{LZ} $100/N$, where $N = 10^6$ is the number of steps in the propagation. We added this number to the corresponding phonon coordinate at the end of the propagation step. The presence of the stochastic term will cause the solutions of the equations of motion to be dependent on the random values generated for each run. We found that solving the equations of motion five times for the same pump amplitude and frequency was enough to assess the probability of each type of solution,

and thus we picked as the solution the one that appeared at least three times for each pair of pump amplitude and frequency values.

In the solutions of the equations of motion, we need to distinguish the translation symmetry breaking due to rectification of the zone-boundary phonon modes from their long-time-period oscillations. Furthermore, since our pump pulses have a finite duration, the dynamics of the phonon coordinates eventually revert to oscillations about their initial equilibrium positions due to the presence of damping terms in the equations of motion. Our criterion for the breaking of translation symmetry is the presence of at least two peaks in the oscillations of Q_{HY} , Q_{LX} , or Q_{LZ} about a displaced position.

III. RESULTS AND DISCUSSION

The lowest-frequency mode of KTaO_3 at X is doubly degenerate. (Check Ref. [40] for the phonon band structure of KTaO_3 .) We follow the notation used in Ref. [41] and call it a TA mode. At a slightly higher frequency, there is a nondegenerate mode that is denoted as longitudinal acoustic. Additionally, there are four doubly degenerate TO and four nondegenerate LO modes, accounting for all 15 phonon modes at X . Figs. 1(top) and (bottom) show the atomic displacements corresponding to the lowest-frequency TA mode Q_{LZ} and highest-frequency LO mode Q_{HY} , respectively. The calculated frequencies of these modes are $\Omega_{\text{LX}} = \Omega_{\text{LZ}} = 61 \text{ cm}^{-1}$ and $\Omega_{\text{HY}} = 843 \text{ cm}^{-1}$, respectively. They agree well with the values inferred from the Raman experiments of Nilsen and Skinner, where these modes appear as peaks at 123 and 1748 cm^{-1} due to the doubling of the respective phonon frequencies in second-order Raman processes [41]. The two components Q_{LZ} and Q_{LX} of the doubly degenerate TA mode belong to the irreducible representation (irrep) X_5^+ , while the LO mode Q_{HY} has the irrep X_3^- . The Q_{LZ} mode involves displacement of the Ta ions against the O octahedra along the z direction. The Q_{HY} mode displaces the pair of O ions situated on the faces of the unit cell parallel to the xy plane against the K ion in the y direction (though the displacement of the K ion is so small that it is not perceptible in the figure), while the rest of the O ions remain stationary. The atomic displacements within the adjacent unit cells are out of phase along the y direction because these modes have the wave vector $(0, \frac{1}{2}, 0)$. They thus break the translation symmetry of the crystal.

Previously, we found that the energy curve of the highest-frequency TO mode at X of KTaO_3 stiffens in the presence of a finite electric field, indicating the presence of a $Q_{\text{HY}}^2 E^2$ nonlinear coupling with a positive coefficient between the phonon coordinate and electric field [27]. When we performed similar total-energy calculations as a function of the highest-frequency LO mode Q_{HY} for different values of the electric field E , we found a softening of the energy curve of the phonon coordi-

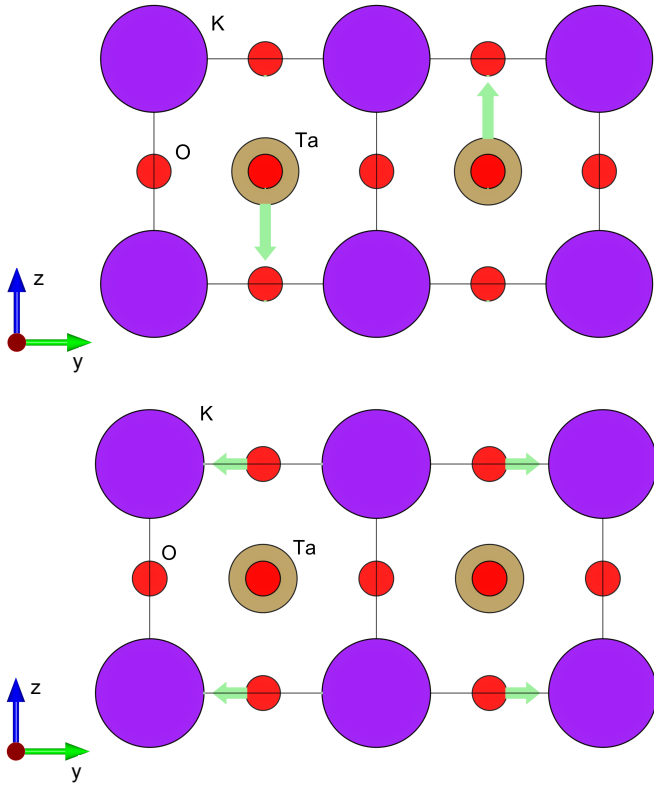


FIG. 1. Atomic displacements due to the phonon modes of KTaO_3 at the X $(0, \frac{1}{2}, 0)$ point considered in the present paper. (Top) The lowest-frequency TA mode component Q_{LZ} that moves Ta ions along the z direction. The other degenerate component of this mode Q_{LX} has the same atomic movements but is directed along the x axis. (Bottom) The highest-frequency LO mode Q_{HY} that causes atomic movements along the y direction.

nate. This softening is symmetric with respect to the sign of both the phonon coordinate ($Q_{HY} \rightarrow -Q_{HY}$) and the electric field ($E \rightarrow -E$), which shows the presence of a $Q_{HY}^2 E^2$ nonlinear coupling with a negative coupling coefficient α . The presence of a $Q_{HY}^2 E^2$ nonlinearity is consistent with the fact that this is the lowest-order coupling term between an electric field and finite-wave-vector phonon allowed by symmetry [42]. However, the negative sign of the coupling coefficient α is surprising. A fit of the total-energy surface $H(Q_{HY}, E)$ by a polynomial gives a relatively small value for the coupling constant $\alpha = -0.205$ e/(V u). Although the magnitude of the coupling constant is small, this in principle makes it possible to break the translation symmetry of the crystal by destabilizing the pumped phonon mode itself. This is illustrated by Fig. 2, which shows the development of symmetrical minima at $Q_{HY} \neq 0$ for an extrapolated electric field of $E = 380$ MV/cm. In order to break the translation symmetry for values of the electric field around 10 MV/cm, we need $\alpha \approx 150$ e/(V u). When the Q_{HY} coordinate is externally pumped, it experiences a force $-\partial H/\partial Q_{HY}$ that leads to a pump-induced renormaliza-

tion of its frequency $\Omega_{HY}^2 \rightarrow \Omega_{HY}^2(1 + 2\alpha E^2)$. Since the correction due to the electric field has an even power, the softening is not averaged out over time, and the Q_{HY} coordinate becomes unstable for $E > \frac{1}{\sqrt{2\alpha}}$.

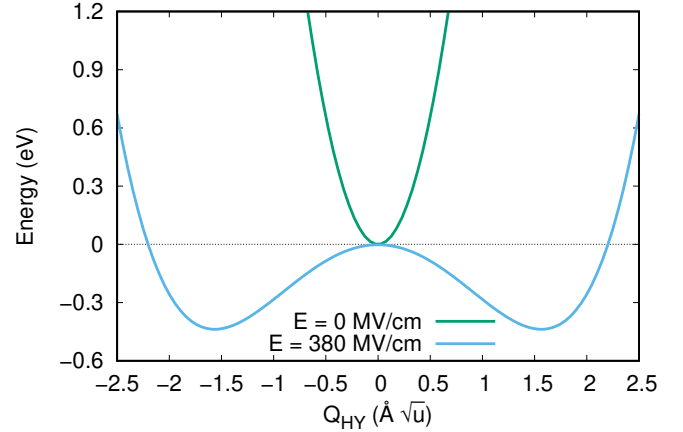


FIG. 2. Total energy as a function of the highest-frequency Q_{HY} phonon coordinate for electric field $E = 0$ and 380 MV/cm.

The pumped energy to the Q_{HY} coordinate should also flow to the lowest-frequency phonon mode at X . To make our paper more realistic, we include the dynamics of the Q_{LZ} and Q_{LX} components of the TA mode in our simulations. Fig. 3 shows five energy curves from the calculated energy surface $V(Q_{HY}, Q_{LX} = 0, Q_{LZ})$. We can again see that the energy curves are symmetric upon the transformations $Q_{LZ} \rightarrow -Q_{LZ}$ and $Q_{HY} \rightarrow -Q_{HY}$, which implies that the energy surface is an even function of both Q_{LZ} and Q_{HY} . Therefore, only terms with even powers of these coordinates occur in the polynomial fit of the total-energy surface. The fact that these modes belong to different irreps imposes this constraint. Since both the Q_{LX} and Q_{LZ} TA components have the same irrep, the same reasoning can be applied to the energy surface $V(Q_{HY}, Q_{LX}, Q_{LZ} = 0)$ and its polynomial fit.

The energy curve of the Q_{LZ} coordinate softens and develops a double-well shape as the magnitude of the Q_{HY} coordinate is increased. Accordingly, the fit of $V(Q_{HY}, Q_{LX} = 0, Q_{LZ})$ yields negative sign for the coefficients of the nonlinear coupling terms $h_1 Q_{HY}^2 Q_{LZ}^2$, $h_2 Q_{HY}^4 Q_{LZ}^2$, and $h_4 Q_{HY}^6 Q_{LZ}^2$ (see Appendix B). The total force experienced along the Q_{LZ} coordinate is given by $-\partial V/\partial Q_{LZ}$, and the nonlinear terms cause a renormalization of its frequency as $\Omega_{LZ}^2 \rightarrow \Omega_{LZ}^2(1 + 2h_1 Q_{HY}^2 + 2h_2 Q_{HY}^4 + 2h_4 Q_{HY}^6 + \dots)$. Only even powers of Q_{HY} appear in this correction. Hence, the softening of the frequency of the Q_{LZ} coordinate due to the oscillation of the Q_{HY} coordinate will not be averaged out over time. The same softening should also occur for the Q_{LX} coordinate because both components of the lowest-frequency TA mode have the same irrep.

We used the calculated total-energy surfaces as the po-

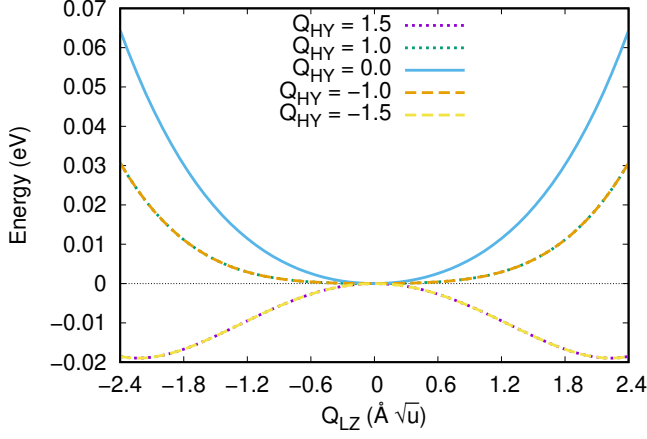


FIG. 3. Calculated total energy as a function of the lowest-frequency TA coordinate Q_{LZ} for different values of the highest-frequency LO coordinate Q_{HY} . For visual clarity, the zero energy point has been chosen so that the curves coincide at $Q_{LZ} = 0$.

tential energy of the Q_{HY} , Q_{LX} , and Q_{LZ} coordinates and used them to construct their coupled equations of motion, which read

$$\begin{aligned} \ddot{Q}_{HY} + \gamma_{HY}\dot{Q}_{HY} + \Omega_{HY}^2 Q_{HY} &= -\frac{\partial V^{nh}(Q_{HY}, Q_{LX}, Q_{LZ})}{\partial Q_{HY}} \\ &+ F(t), \\ \ddot{Q}_{LX} + \gamma_{LX}\dot{Q}_{LX} + \Omega_{LX}^2 Q_{LX} &= -\frac{\partial V^{nh}(Q_{HY}, Q_{LX}, Q_{LZ})}{\partial Q_{LX}}, \\ \ddot{Q}_{LZ} + \gamma_{LZ}\dot{Q}_{LZ} + \Omega_{LZ}^2 Q_{LZ} &= -\frac{\partial V^{nh}(Q_{HY}, Q_{LX}, Q_{LZ})}{\partial Q_{LZ}}. \end{aligned} \quad (2)$$

Here $V^{nh}(Q_{HY}, Q_{LX}, Q_{LZ})$ is the nonharmonic part of the polynomial fit to the calculated total-energy surfaces as a function of the three coordinates. Its full expression is given in Appendix B. The damping coefficients γ_i are set to 10% of the value of their corresponding natural frequency. The external force $F(t)$ experienced by the Q_{HY} coordinate due to its coupling with the electric field of the pump pulse is given by

$$F = -\frac{\partial H(Q_{HY}, E)}{\partial Q_{HY}} = -2\alpha Q_{HY} E^2. \quad (3)$$

Since pulsed laser sources with finite time duration are used in most pump-probe experiments, we studied the dynamics using Gaussian-enveloped single-frequency pulses for the electric field

$$E_{sf}(t) = E_0 \sin(\omega t) e^{-t^2/2(\sigma/2\sqrt{2\log 2})^2}. \quad (4)$$

Here E_0 , ω , and σ are the amplitude, frequency, and duration (full width at half maximum) of the pulse, respectively. We used $\sigma = 2$ ps in all our simulations. Chirped

laser sources are also used in pump-probe experiments, and we have repeated our simulations with Gaussian-enveloped chirped pulses. These results are presented in Appendix A, as they were analogous to those obtained with the single-frequency pulse but with a slightly lower threshold for the pulse amplitude that manages to achieve rectification of the phonon coordinates.

For a given value of pump frequency, we solved the coupled equations of motion of the Q_{HY} , Q_{LX} , and Q_{LZ} coordinates given in Eq. 2 for a range of pump amplitude E_0 . When the pump amplitude is small, the pumped mode Q_{HY} oscillates at its natural frequency Ω_{HY} without getting amplified and decays at a rate determined by γ_{HY} . Hence, the energy transferred to the Q_{LZ} and Q_{LX} coordinates is also small, and they also briefly oscillate at their natural frequencies $\Omega_{LZ} = \Omega_{LX}$ without getting amplified. At the other extreme, all three modes diverge at very large values of the the pump amplitude, which corresponds to the dielectric breakdown of the material. In between these uninteresting scenarios, we searched for a range of pump frequency and amplitude where at least one of the three coordinates oscillates at a displaced position.

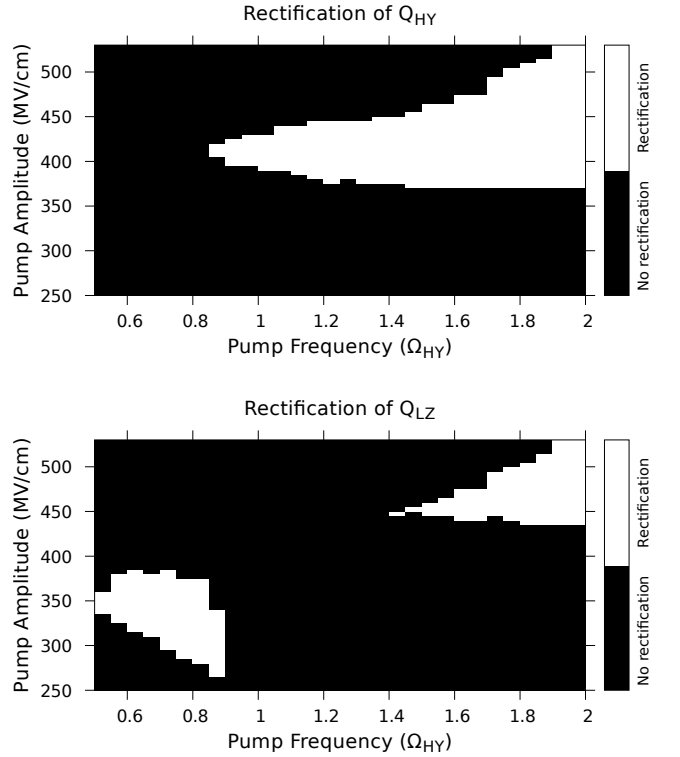


FIG. 4. Pump amplitudes and frequencies of the single-frequency pulse driving the Q_{HY} phonon coordinate that induce rectification of the Q_{HY} (top) and Q_{LZ} (bottom) coordinates. As both components of the lowest-frequency TA mode have the same irrep, the results for the Q_{LX} coordinate are analogous to those of Q_{LZ} .

We find that for very low pump frequencies the ef-

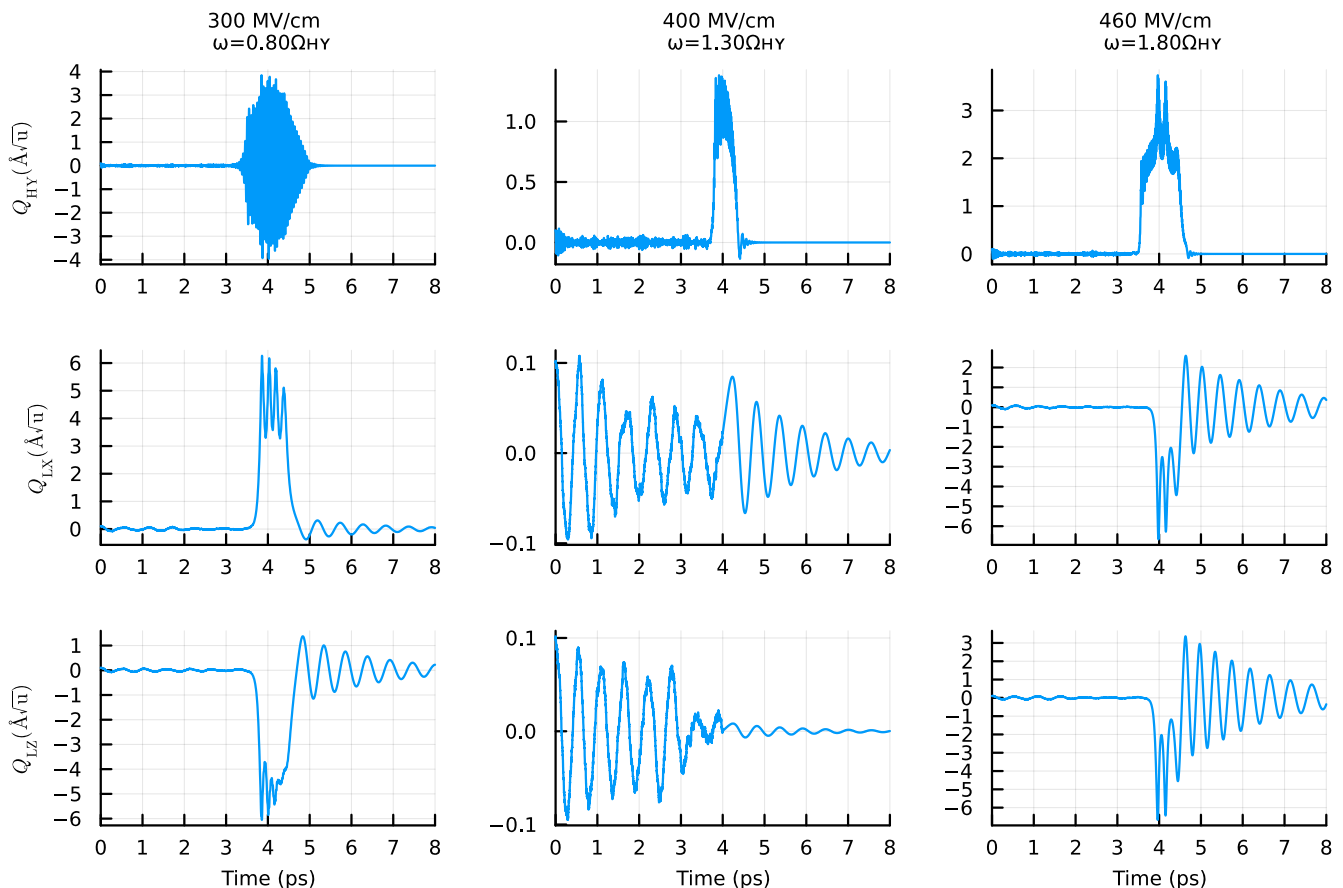


FIG. 5. Examples of the three rectification regimes of the Q_{HY} , Q_{LX} , and Q_{LZ} phonon coordinates for pump pulses with frequencies of $\omega = 0.80\Omega_{\text{HY}}$ (left), $\omega = 1.30\Omega_{\text{HY}}$ (center), and $\omega = 1.80\Omega_{\text{HY}}$ (right) and amplitudes of 300, 400, and 460 MV/cm respectively.

fect of the pump pulse is no different from applying a constant electric field, driving the pumped Q_{HY} mode close to its natural frequency Ω_{HY} for the duration of the pulse. Above pump frequency of $\omega > 0.50\Omega_{\text{HY}}$, we were able to find pump amplitudes for three different types of rectification of the phonon coordinates, which is shown in Fig. 4. For $0.50\Omega_{\text{HY}} < \omega < 0.85\Omega_{\text{HY}}$, the lowest-frequency TA coordinates Q_{LZ} and Q_{LX} get rectified while the pumped Q_{HY} mode oscillates at its equilibrium position. Interestingly, in the range $0.85\Omega_{\text{HY}} < \omega < 1.40\Omega_{\text{HY}}$, the pumped mode Q_{HY} itself oscillates at a displaced position while the oscillations of the lowest-frequency TA coordinates occur about their equilibrium positions. Finally, at $\omega > 1.40\Omega_{\text{HY}}$ all three coordinates get rectified.

The rectification of the lowest-frequency Q_{LZ} and Q_{LX} coordinates for values of pump frequencies in the window $0.50\Omega_{\text{HY}} < \omega < 0.85\Omega_{\text{HY}}$ is similar to the behavior obtained by us in our previous work where the highest-frequency TO mode was externally pumped [27]. The rectification occurs because they experience a time-averaged double-well potential while the high-frequency LO coordinate Q_{HY} oscillates around its equilibrium po-

sition with a large enough amplitude. At a pump frequency of $\omega = 0.50\Omega_{\text{HY}}$, we find that the earliest onset of the rectification of the TA modes occurs for a pump amplitude of 335 MV/cm. Smaller amplitudes do not excite the LO mode enough to induce the rectification of the TA modes, and amplitudes larger than 350 MV/cm cause the TA modes to quickly oscillate between the two wells of the potential with a time average of zero. As the pump frequency is increased within the window of this regime, the TA modes start getting rectified at lower pump amplitudes, while the solution of the equations of motion starts to diverge as the pump amplitude is increased above 380 MV/cm. As a result, the range of amplitudes that induce the rectification of the TA coordinates broadens with the frequency of the pump pulse until a new regime is reached above pump frequency of $\omega > 0.85\Omega_{\text{HY}}$. This behavior is reflected in the left areas of Figs. 4 (top) and (bottom). The left column of Fig. 5 shows the time evolutions of the three coordinates for a pump frequency of $\omega = 0.80\Omega_{\text{HY}}$ and amplitude of 300 MV/cm, which is a representative solution of the equations of motion in this regime. They exhibit rectification of the TA coordinates with $\langle Q_{\text{LZ}} \rangle$ and $\langle Q_{\text{LX}} \rangle \neq 0$, while

the LO coordinate oscillates about the equilibrium position with $\langle Q_{\text{HY}} \rangle = 0$. Surprisingly, we find that that the time-averaged position about which the TA coordinates oscillate at a displaced position does not change as a function of the pump amplitude in this regime.

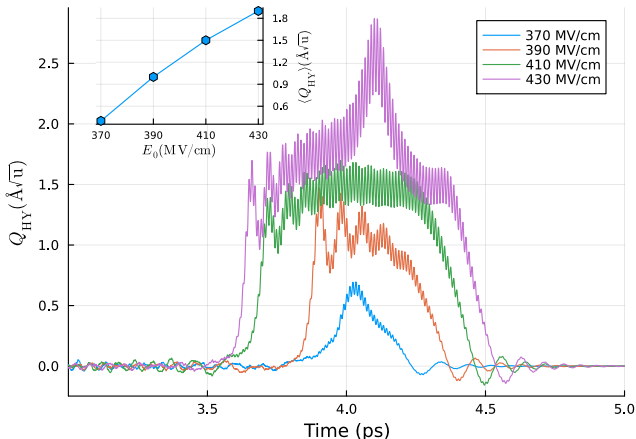


FIG. 6. Growth of the rectified position of the Q_{HY} phonon coordinate as a function of the amplitude of the pump. The frequency of the pulse was set to $\omega = 1.80\Omega_{\text{HY}}$, where $\Omega_{\text{HY}} = 843 \text{ cm}^{-1}$. Inset: The average position $\langle Q_{\text{HY}} \rangle$ during the rectification as a function of the peak amplitude of the applied electric field E_0 . The line connecting the dots is a guide for the eye.

For values of pump frequency in the window $0.85\Omega_{\text{HY}} < \omega < 1.40\Omega_{\text{HY}}$, we find a regime where the pumped LO mode Q_{HY} is rectified but the lowest-frequency TA components remain oscillating around their equilibrium position. Interestingly, the amplitude of the pumped coordinate Q_{HY} drops significantly upon entering this regime. An example of the time evolutions of the three phonon coordinates in this regime is shown in the middle column of Fig. 5, which was obtained for a pump frequency $\omega = 1.30\Omega_{\text{HY}}$ and amplitude $E_0 = 400 \text{ MV/cm}$. Instead of oscillating about the equilibrium position, the pumped mode gets rectified because of the negative sign of the coefficient α of the quartic-order $Q_{\text{HY}}^2 E^2$ light-phonon coupling term. For a pump frequency $\omega = 0.85\Omega_{\text{HY}}$ that is near the beginning of this window, the rectification of the LO mode happens for pump amplitudes from 405 to 415 MV/cm. As the pump frequency is increased, the range of the pump amplitude that rectifies the Q_{HY} mode broadens. For a pump frequency of $\omega = 1.40\Omega_{\text{HY}}$, this range goes from 375 to 440 MV/cm, as we can see on the top panel of Fig. 4. Larger values of pump amplitude cause the equations of motion to diverge, signaling the breakdown of the material. However, until the divergence occurs, the new position about which the rectified oscillations of the Q_{HY} mode occurs increases with the amplitude of the pump in approximately linear fashion. This is illustrated in Fig. 6, which shows the time evolution of Q_{HY} for four increasing values of pump amplitude. This change in the displaced

position of the Q_{HY} coordinate is different from the almost unchanged rectified position of the TA coordinates discussed in the previous paragraph.

When pump frequency is in the range $0.85\Omega_{\text{HY}} < \omega < 1.40\Omega_{\text{HY}}$, the values reached by the rectified Q_{HY} coordinate are not large enough to induce a rectification of the TA modes through their phonon-phonon coupling before the divergence of the equations of motion. However, for pump frequencies $\omega > 1.40\Omega_{\text{HY}}$, the values reached by the pumped coordinate Q_{HY} start to be comparable to that reached by it in the first regime, and we enter a distinct regime where we can find pump amplitudes that can rectify the three modes at the same time. At pump frequency $\omega = 1.45\Omega_{\text{HY}}$, pump amplitudes between 370 and 440 MV/cm cause rectification of the LO mode without rectifying the TA mode, as discussed above. But when the pump amplitude is increased above 440 MV/cm, the oscillation about the transient displaced position of the Q_{HY} coordinate is large enough to induce rectification of the Q_{LZ} and Q_{LX} TA coordinates. This behavior has an activation threshold for the pump amplitude of 440 MV/cm, but the maximum amplitude that manages to induce this triple rectification without causing the breakdown of the material grows linearly with the frequency until reaching a plateau of around 530 MV/cm starting at $\omega = 1.90\Omega_{\text{HY}}$. An example of the time evolution of the three coordinates in this regime is shown in the right column of Fig. 5. One notable feature of this regime is that the Q_{HY} mode beats at the same frequency as the Q_{LZ} and Q_{LX} modes, suggesting that the energy that flows to the TA coordinates dominates the dynamics of the system.

IV. SUMMARY AND CONCLUSIONS

In summary, we have discovered using first principles total-energy calculations that a quartic-order $\alpha Q_{\text{HY}}^2 E^2$ coupling with a negative coefficient α occurs between the highest-frequency LO phonon coordinate Q_{HY} of KTaO_3 at the Brillouin zone boundary point X and electric field E . This implies that the Q_{HY} mode softens when it is driven by an external laser source. We investigated the feasibility of transiently breaking the translation symmetry of KTaO_3 by driving the Q_{HY} mode to instability using pump pulses with high electric field. We also considered the coupling of the Q_{HY} mode with the lowest-frequency TA phonon modes Q_{LZ} and Q_{LX} at X . The nonlinear couplings between these modes were also obtained from first principles by calculating the total energy as a function of the phonon coordinates. We find that the energy curves of the TA coordinates Q_{LZ} and Q_{LX} develop a double-well shape for finite values of the Q_{HY} coordinate, suggesting that these modes could also become unstable when the Q_{HY} is externally pumped. We used the calculated nonlinear couplings to construct the coupled equations of motion for the three coordinates in the presence of a Gaussian-enveloped pump pulse term

on the Q_{HY} mode. These were then numerically solved for a range of pump frequencies and amplitudes.

We find three different regimes of light-induced translation symmetry breaking, which occur for pump frequency $\omega > 0.5\Omega_{\text{HY}}$ when a Gaussian-enveloped single-frequency pump pulse is used. Only the TA coordinates Q_{LZ} and Q_{LX} rectify when pump frequency is in the range $0.5 < \omega < 0.85\Omega_{\text{HY}}$. The lowest pump amplitude that can cause rectification in this regime is 270 MV/cm. When pump frequency is in the range $0.85 < \omega < 1.40\Omega_{\text{HY}}$, only the pumped mode Q_{HY} rectifies. A pump amplitude of at least 375 MV/cm is required to exhibit this behavior. Finally, all three coordinates can rectify when the pump frequency is greater than $1.40\Omega_{\text{HY}}$, which requires a pump amplitude of at least 440 MV/cm. We find that the use of chirped pulses only modestly decreases the threshold required to rectify these modes.

The pump amplitude required to break the translation symmetry of KTaO_3 by pumping its highest-frequency LO coordinate is well beyond what can be produced by currently available experimental setups. Even if powerful laser sources were available, such intense pump pulses would likely cause dielectric breakdown of the sample. Nevertheless, we have shown that quartic-order light-phonon coupling with negative sign can occur in real materials that can be utilized to break the translation symmetry of the crystal by rectifying the pumped mode. Our paper motivates the search for materials where the magnitude of this light-phonon coupling is large.

ACKNOWLEDGMENTS

This work was supported by the Agence Nationale de la Recherche under grant ANR-19-CE30-0004 ELECTROPHONE and GENCI-TGCC under grant A0110913028.

APPENDIX A: CHIRPED PULSE

Chirped pulses can be more effective at driving the phonon modes of a material, especially if the pumped mode transiently hardens [43]. We also studied the light-induced dynamics of the three phonon coordinates described by Eqs. 2 using Gaussian-enveloped chirped pulses having electric field

$$E_{\text{ch}}(t) = E_0 \sin(\beta t^2) e^{-t^2/2(\sigma/2\sqrt{2\log 2})^2}. \quad (\text{A1})$$

Here, β is the chirp parameter that describes the linear growth of the pulse as a function of time.

Fig. 7 shows the values of the amplitude and β of the pump pulse that manage to induce the rectification of the phonon modes. We find that the effect of the chirped pulse is similar to applying a constant electric field for the growth rate of the frequency $\beta < 1.5$ THz/ps, the same situation we found when using single-frequency pump pulses with frequencies below $0.50\Omega_{\text{HY}}$.

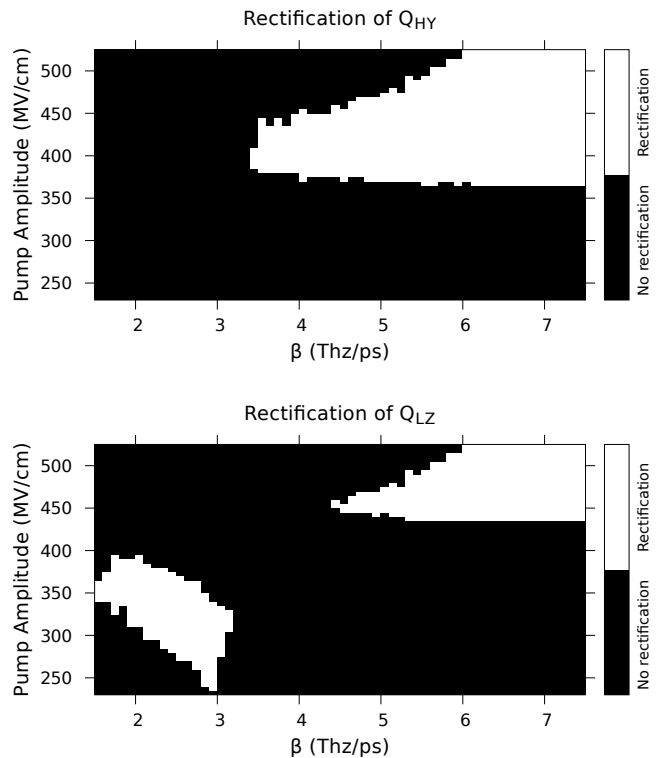


FIG. 7. Pump amplitudes and frequency-growth rate parameters β of the chirped pulse driving the Q_{HY} phonon coordinate that induce a rectification of the Q_{HY} (top) and Q_{LZ} (bottom) coordinates. As both components of the lowest-frequency TA mode have the same irrep, the results for the Q_{LX} mode are analogous to those of Q_{LZ} .

Above $\beta > 1.5$ THz/ps, we can distinguish the same three regimes that we found for the single-frequency pulse: (i) rectification of the lowest-frequency TA coordinates Q_{LZ} and Q_{LX} , (ii) rectification of the pumped LO coordinate Q_{HY} , and (iii) rectification of all three coordinates. The rectification of only the TA coordinates happens for $1.5 < \beta < 3.1$ THz/ps. The lowest value of the pump amplitude that causes rectification in this regime is 235 MV/cm, which occurs for $\beta = 2.9$ THz/ps. This is slightly smaller than the value of 270 MV/cm obtained for a single-frequency pulse. For values of the chirp parameter $\beta > 3.4$ THz/ps, we can find pump amplitudes that rectify the pumped phonon coordinate Q_{HY} . The lowest pump amplitude that rectifies Q_{HY} is 385 MV/cm at $\beta = 3.4$ THz/ps. This threshold decreases as β is increased until $\beta = 6.1$ THz/ps, where it stabilizes at 365 MV/cm. For comparison, the lowest pump value to cause rectification of Q_{HY} using single-frequency pulse is 370 MV/cm. Only the pumped LO coordinate Q_{HY} gets rectified for $3.4 < \beta < 4.4$ THz/ps, whereas pump amplitudes that cause rectification of all three coordinates can be found for $\beta > 4.4$ THz/ps. An example of each regime is plotted in Fig. 8.

The results obtained using the chirped pump pulse

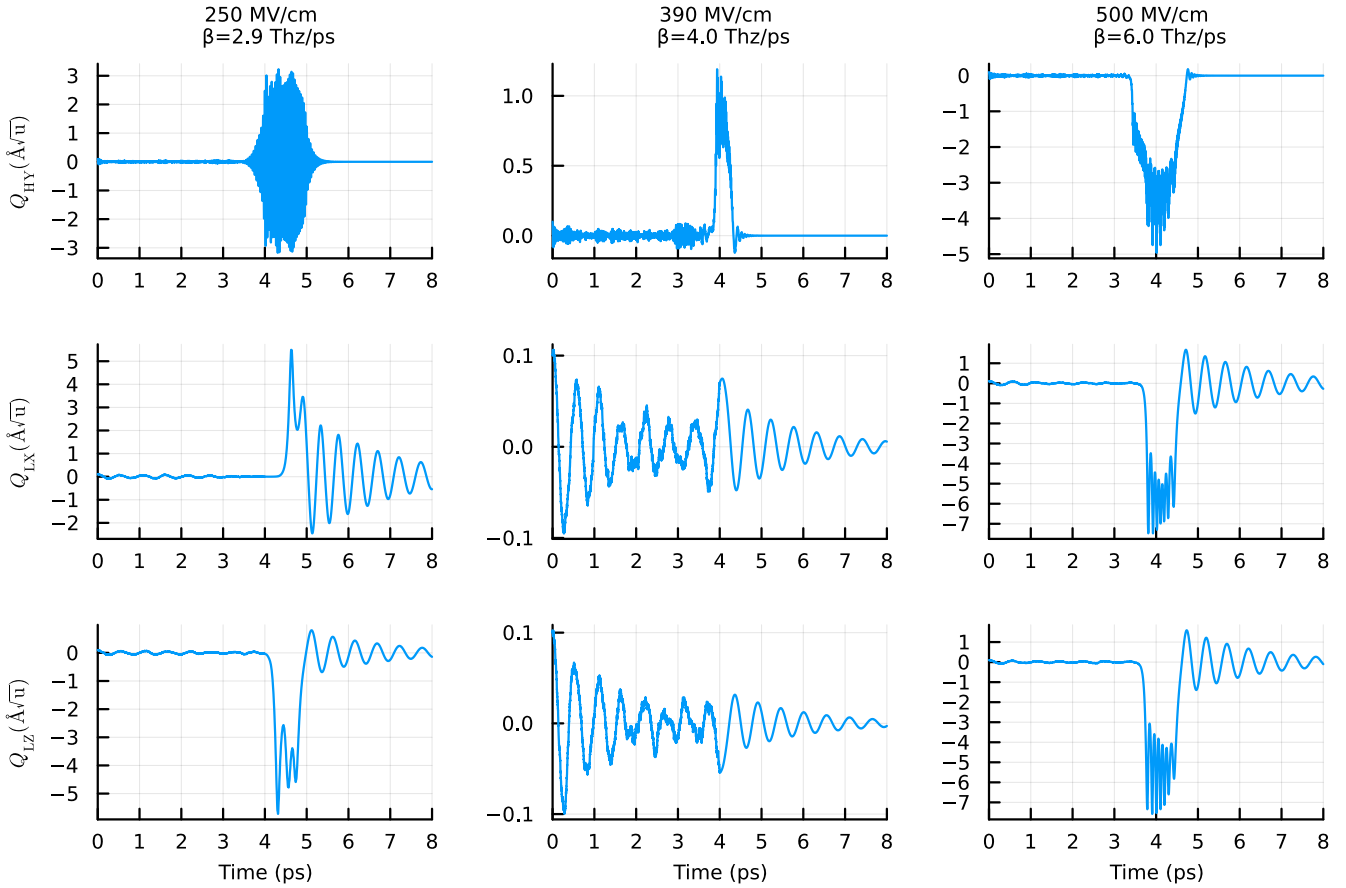


FIG. 8. Examples of the three rectification regimes of the Q_{HY} , Q_{LX} , and Q_{LZ} phonon coordinates for chirped pulses with frequency-growth rate parameters of $\beta = 2.9$ Thz/ps (left), $\beta = 4.0$ Thz/ps (center), and $\beta = 6.0$ Thz/ps (right) and amplitudes of 250, 390, and 500 MV/cm respectively.

are analogous to those found for the single-frequency pulse, except for the slightly smaller threshold value of the pump pulse amplitude that causes rectification of the phonon coordinates. The efficiency of the pump increases because the chirped pulse includes a wider range of fre-

quencies. The frequency of the pumped LO mode stiffens while it is driven to large-amplitude oscillations due to the presence of anharmonic terms. Hence, a pulse that is capable of matching this changing frequency is more efficient at exciting the phonon mode than the single-frequency one.

APPENDIX B: EXPRESSION FOR THE TOTAL ENERGY SURFACE

As in our previous work [27], the phonon anharmonicities and phonon-phonon couplings between the three coordinates Q_{HY} , Q_{LZ} , and Q_{LX} were obtained by fitting the calculated total-energy surface $V(Q_{\text{HY}}, Q_{\text{LX}}, Q_{\text{LZ}})$ with the following expression

$$V = \frac{1}{2}\Omega_{\text{LX}}^2 Q_{\text{LX}}^2 + \frac{1}{2}\Omega_{\text{LZ}}^2 Q_{\text{LZ}}^2 + \frac{1}{2}\Omega_{\text{HY}}^2 Q_{\text{HY}}^2 + V^{\text{nh}}, \quad (\text{B1})$$

where the nonharmonic part $V^{\text{nh}}(Q_{\text{HY}}, Q_{\text{LX}}, Q_{\text{LZ}})$ is given by

$$\begin{aligned}
V^{\text{nh}} = & a_4 Q_{\text{LX}}^4 + a_6 Q_{\text{LX}}^6 + a_8 Q_{\text{LX}}^8 + b_4 Q_{\text{LZ}}^4 + b_6 Q_{\text{LZ}}^6 + b_8 Q_{\text{LZ}}^8 + d_4 Q_{\text{HY}}^4 + d_6 Q_{\text{HY}}^6 + d_8 Q_{\text{HY}}^8 \\
& + e_1 Q_{\text{LX}}^2 Q_{\text{LZ}}^2 + e_2 Q_{\text{LX}}^4 Q_{\text{LZ}}^2 + e_3 Q_{\text{LX}}^2 Q_{\text{LZ}}^4 + e_4 Q_{\text{LX}}^6 Q_{\text{LZ}}^2 + e_5 Q_{\text{LX}}^4 Q_{\text{LZ}}^4 + e_6 Q_{\text{LX}}^2 Q_{\text{LZ}}^6 \\
& + h_1 Q_{\text{HY}}^2 Q_{\text{LX}}^2 + h_2 Q_{\text{HY}}^4 Q_{\text{LX}}^2 + h_3 Q_{\text{HY}}^2 Q_{\text{LX}}^4 + h_4 Q_{\text{HY}}^6 Q_{\text{LX}}^2 + h_5 Q_{\text{HY}}^4 Q_{\text{LX}}^4 + h_6 Q_{\text{HY}}^2 Q_{\text{LX}}^6 \\
& + i_1 Q_{\text{HY}}^2 Q_{\text{LZ}}^2 + i_2 Q_{\text{HY}}^4 Q_{\text{LZ}}^2 + i_3 Q_{\text{HY}}^2 Q_{\text{LZ}}^4 + i_4 Q_{\text{HY}}^6 Q_{\text{LZ}}^2 + i_5 Q_{\text{HY}}^4 Q_{\text{LZ}}^4 + i_6 Q_{\text{HY}}^2 Q_{\text{LZ}}^6 \\
& + k_1 Q_{\text{HY}}^2 Q_{\text{LX}}^2 Q_{\text{LZ}}^2 + k_2 Q_{\text{HY}}^4 Q_{\text{LX}}^2 Q_{\text{LZ}}^2 + k_3 Q_{\text{HY}}^2 Q_{\text{LX}}^4 Q_{\text{LZ}}^2 + k_4 Q_{\text{HY}}^2 Q_{\text{LX}}^2 Q_{\text{LZ}}^4.
\end{aligned} \tag{B2}$$

The values of the coefficients extracted from the fit are given in Table I.

TABLE I. The harmonic, anharmonic, and nonlinear coupling terms extracted from the polynomial fit of the calculated total-energy surface $V(Q_{\text{HY}}, Q_{\text{LX}}, Q_{\text{LZ}})$ of KTAO_3 . The units are $\text{eV}/(\text{\AA}\sqrt{\text{u}})^{i+j+k}$, where i, j and k are the exponents of the phonon coordinates.

Coefficient	Order	Value	Coefficient	Order	Value
Ω_{LX}^2	Q_{LX}^2	0.013628	e_6	$Q_{\text{LX}}^2 Q_{\text{LZ}}^6$	1.96×10^{-7}
Ω_{LZ}^2	Q_{LZ}^2	0.013628	h_1	$Q_{\text{HY}}^2 Q_{\text{LX}}^2$	-5.4947×10^{-3}
Ω_{HY}^2	Q_{HY}^2	2.612711	h_2	$Q_{\text{HY}}^4 Q_{\text{LX}}^2$	-4.27×10^{-4}
a_4	Q_{LX}^4	7.99×10^{-4}	h_3	$Q_{\text{HY}}^2 Q_{\text{LX}}^4$	1.068×10^{-5}
a_6	Q_{LX}^6	-8.6×10^{-6}	h_4	$Q_{\text{HY}}^6 Q_{\text{LX}}^2$	-5.59×10^{-6}
a_8	Q_{LX}^8	1.93×10^{-7}	h_5	$Q_{\text{HY}}^4 Q_{\text{LX}}^4$	9.9×10^{-7}
b_4	Q_{LZ}^4	7.99×10^{-4}	h_6	$Q_{\text{HY}}^2 Q_{\text{LX}}^6$	2.5×10^{-7}
b_6	Q_{LZ}^6	-8.6×10^{-6}	i_1	$Q_{\text{HY}}^2 Q_{\text{LZ}}^2$	-5.4947×10^{-3}
b_8	Q_{LZ}^8	1.93×10^{-7}	i_2	$Q_{\text{HY}}^4 Q_{\text{LZ}}^2$	-4.27×10^{-4}
d_4	Q_{HY}^4	0.06897	i_3	$Q_{\text{HY}}^2 Q_{\text{LZ}}^4$	1.068×10^{-5}
d_6	Q_{HY}^6	7.8×10^{-4}	i_4	$Q_{\text{HY}}^6 Q_{\text{LZ}}^2$	-5.59×10^{-6}
d_8	Q_{HY}^8	-1.1×10^{-5}	i_5	$Q_{\text{HY}}^4 Q_{\text{LZ}}^4$	9.9×10^{-7}
e_1	$Q_{\text{LX}}^2 Q_{\text{LZ}}^2$	2.796×10^{-4}	i_6	$Q_{\text{HY}}^2 Q_{\text{LZ}}^6$	2.5×10^{-7}
e_2	$Q_{\text{LX}}^4 Q_{\text{LZ}}^2$	-1.14×10^{-5}	k_1	$Q_{\text{HY}}^2 Q_{\text{LX}}^2 Q_{\text{LZ}}^2$	3.83×10^{-5}
e_3	$Q_{\text{LX}}^2 Q_{\text{LZ}}^4$	-1.14×10^{-5}	k_2	$Q_{\text{HY}}^4 Q_{\text{LX}}^2 Q_{\text{LZ}}^2$	6.1×10^{-6}
e_4	$Q_{\text{LX}}^6 Q_{\text{LZ}}^2$	1.96×10^{-7}	k_3	$Q_{\text{HY}}^2 Q_{\text{LX}}^4 Q_{\text{LZ}}^2$	-3.6×10^{-7}
e_5	$Q_{\text{LX}}^4 Q_{\text{LZ}}^4$	2.35×10^{-7}	k_4	$Q_{\text{HY}}^2 Q_{\text{LX}}^2 Q_{\text{LZ}}^4$	-3.6×10^{-7}

- [1] S. R. Ovshinsky, Physical review letters **21**, 1450 (1968).
- [2] L. Stojchevska, I. Vaskivskiy, T. Mertelj, P. Kusar, D. Svetin, S. Brazovskii, and D. Mihailovic, Science **344**, 177 (2014).
- [3] M. Först, C. Manzoni, S. Kaiser, Y. Tomioka, Y. Tokura, R. Merlin, and A. Cavalleri, Nature Physics **7**, 854 (2011).
- [4] A. Subedi, Phys. Rev. B **92**, 214303 (2015).
- [5] R. Mankowsky, A. von Hoegen, M. Först, and A. Cavalleri, Phys. Rev. Lett. **118**, 197601 (2017).
- [6] M. Henstridge, M. Först, E. Rowe, M. Fechner, and A. Cavalleri, Nature Physics **18**, 457 (2022).
- [7] T. Mertelj and V. V. Kabanov, Phys. Rev. Lett. **123**, 129701 (2019).
- [8] V. A. Abalmasov, Phys. Rev. B **101**, 014102 (2020).
- [9] P. Chen, C. Paillard, H. J. Zhao, J. Íñiguez, and L. Bellaiche, Nature Communications **13**, 2566 (2022).
- [10] A. Subedi, A. Cavalleri, and A. Georges, Phys. Rev. B **89**, 220301 (2014).
- [11] A. Subedi, Phys. Rev. B **95**, 134113 (2017).
- [12] P. G. Radaelli, Physical Review B **97**, 085145 (2018).
- [13] A. Melnikov, Y. G. Selivanov, and S. Chekalin, Physical Review B **102**, 224301 (2020).
- [14] M. Gu and J. M. Rondinelli, Scientific reports **6**, 25121 (2016).
- [15] D. M. Juraschek, M. Fechner, A. V. Balatsky, and N. A. Spaldin, Physical Review Materials **1**, 014401 (2017).
- [16] M. Fechner, A. Sukhov, L. Chotorlishvili, C. Kenel, J. Berakdar, and N. Spaldin, Physical review materials **2**, 064401 (2018).
- [17] G. Khalsa and N. A. Benedek, npj Quantum Materials **3**, 1 (2018).
- [18] M. Gu and J. M. Rondinelli, Physical Review B **98**, 024102 (2018).
- [19] M. Rodriguez-Vega, Z.-X. Lin, A. Leonardo, A. Ernst, M. G. Vergniory, and G. A. Fiete, The Journal of Physical Chemistry Letters **13**, 4152 (2022).
- [20] D. M. Juraschek, T. Neuman, and P. Narang, Physical Review Research **4**, 013129 (2022).
- [21] N. Feng, J. Han, C. Lan, B. Xu, K. Bi, Y. Lin, and C. Nan, Physical Review B **105**, 024304 (2022).
- [22] T. F. Nova, A. Cartella, A. Cantaluppi, M. Först, D. Bossini, R. V. Mikhaylovskiy, A. V. Kimel, R. Merlin, and A. Cavalleri, Nature Physics **13**, 132 (2017).

- [23] A. S. Disa, M. Fechner, T. F. Nova, B. Liu, M. Först, D. Prabhakaran, P. G. Radaelli, and A. Cavalleri, *Nature Physics* **16**, 937 (2020).
- [24] A. Stupakiewicz, C. Davies, K. Szerenos, D. Afanasiev, K. Rabinovich, A. Boris, A. Caviglia, A. Kimel, and A. Kirilyuk, *Nature Physics* **17**, 489 (2021).
- [25] D. Afanasiev, J. Hortensius, B. Ivanov, A. Sasani, E. Bousquet, Y. Blanter, R. Mikhaylovskiy, A. Kimel, and A. Caviglia, *Nature materials* **20**, 607 (2021).
- [26] A. S. Disa, J. Curtis, M. Fechner, A. Liu, A. von Hoegen, M. Först, T. F. Nova, P. Narang, A. Maljuk, A. V. Boris, B. Keimer, and A. Cavalleri, *Nature* **617**, 73 (2023).
- [27] A. Gómez Pueyo and A. Subedi, *Phys. Rev. B* **106**, 214305 (2022).
- [28] A. Subedi, *Comptes Rendus. Physique* **22**, 161 (2021).
- [29] A. Cartella, T. F. Nova, M. Fechner, R. Merlin, and A. Cavalleri, *Proceedings of the National Academy of Sciences* **115**, 12148 (2018), <https://www.pnas.org/content/115/48/12148.full.pdf>.
- [30] P. Giannozzi, O. Baseggio, P. Bonfà, D. Brunato, R. Car, I. Carnimeo, C. Cavazzoni, S. de Gironcoli, P. Delugas, F. Ferrari Ruffino, A. Ferretti, N. Marzari, I. Timrov, A. Urru, and S. Baroni, *The Journal of Chemical Physics* **152**, 154105 (2020), <https://doi.org/10.1063/5.0005082>.
- [31] J. P. Perdew, A. Ruzsinszky, G. I. Csonka, O. A. Vydrov, G. E. Scuseria, L. A. Constantin, X. Zhou, and K. Burke, *Phys. Rev. Lett.* **100**, 136406 (2008).
- [32] K. F. Garrity, J. W. Bennett, K. M. Rabe, and D. Vanderbilt, *Computational Materials Science* **81**, 446 (2014).
- [33] S. Y. Savrasov, D. Y. Savrasov, and O. K. Andersen, *Phys. Rev. Lett.* **72**, 372 (1994).
- [34] K. Sokolowski-Tinten, C. Blome, J. Blums, A. Cavalleri, C. Dietrich, A. Tarasevitch, I. Uschmann, E. Förster, M. Kammler, M. Horn-von Hoegen, and D. von der Linde, *Nature* **422**, 287 (2003).
- [35] D. Bates, S. Kornblith, A. Noack, M. Bouchet-Valat, M. K. Borregaard, A. Arslan, J. M. White, D. Kleinschmidt, G. Lynch, I. Dunning, P. K. Mogensen, S. Lendle, D. Aluthge, pdeffebach, P. José Bayoán Santiago Calderón, B. Born, B. Setzler, C. DuBois, J. Quinn, O. Slámečka, P. Bastide, P. Alday, P. Anthony Blaom, B. König, B. Kamiński, C. Caine, D. Lin, and D. Karasch, *Juliastats/glm.jl: v1.6.0* (2022).
- [36] I. Souza, J. Íñiguez, and D. Vanderbilt, *Phys. Rev. Lett.* **89**, 117602 (2002).
- [37] C. Rackauckas and Q. Nie, *The Journal of Open Research Software* **5** (2017), exported from <https://app.dimensions.ai> on 2019/05/05.
- [38] L. Caprini, H. Löwen, and R. M. Geilhufe, *Ultrafast entropy production in pump-probe experiments* (2023), [arXiv:2302.02716 \[cond-mat.mtrl-sci\]](https://arxiv.org/abs/2302.02716).
- [39] D. M. Juraschek, Q. N. Meier, and P. Narang, *Phys. Rev. Lett.* **124**, 117401 (2020).
- [40] C. H. Perry, R. Currat, H. Buhay, R. M. Migoni, W. G. Stirling, and J. D. Axe, *Phys. Rev. B* **39**, 8666 (1989).
- [41] W. G. Nilsen and J. G. Skinner, *The Journal of Chemical Physics* **47**, 1413 (1967), <https://doi.org/10.1063/1.1712096>.
- [42] A. Bartels, T. Dekorsy, and H. Kurz, *Phys. Rev. Lett.* **84**, 2981 (2000).
- [43] A. Itin and M. Katsnelson, *Physical Review B* **97**, 184304 (2018).